

A Cognitive Particle Filter for Collaborative DGNS Positioning

Original

A Cognitive Particle Filter for Collaborative DGNS Positioning / Minetto, Alex; Gurrieri, Alessandro; Dosis, Fabio. - In: IEEE ACCESS. - ISSN 2169-3536. - ELETTRONICO. - 8:(2020), pp. 194765-194779. [10.1109/ACCESS.2020.3033626]

Availability:

This version is available at: 11583/2851149 since: 2020-11-05T10:33:06Z

Publisher:

Institute of Electrical and Electronics Engineers (IEEE)

Published

DOI:10.1109/ACCESS.2020.3033626

Terms of use:

This article is made available under terms and conditions as specified in the corresponding bibliographic description in the repository

Publisher copyright

IEEE postprint/Author's Accepted Manuscript

©2020 IEEE. Personal use of this material is permitted. Permission from IEEE must be obtained for all other uses, in any current or future media, including reprinting/republishing this material for advertising or promotional purposes, creating new collecting works, for resale or lists, or reuse of any copyrighted component of this work in other works.

(Article begins on next page)

Received September 23, 2020, accepted October 17, 2020, date of publication October 26, 2020, date of current version November 6, 2020.

Digital Object Identifier 10.1109/ACCESS.2020.3033626

A Cognitive Particle Filter for Collaborative DGNSS Positioning

ALEX MINETTO^{ID}, (Member, IEEE), ALESSANDRO GURRIERI,
AND FABIO DOVIS^{ID}, (Member, IEEE)

Department of Electronics and Telecommunication, Politecnico di Torino, 10129 Turin, Italy

Corresponding author: Alex Minetto (alex.minetto@polito.it)

ABSTRACT The advances in low-latency communications networks and the ever-growing amount of devices offering localization and navigation capabilities opened a number of opportunities to develop innovative network-based collaborative solutions to satisfy the increasing demand for positioning accuracy and precision. Recent research works indeed, have fostered the concept of networked Global Navigation Satellite System (GNSS) receivers supporting the sharing of raw measurements with other receivers within the same network. Such measurements (i.e. pseudorange and Doppler) can be processed through Differential GNSS (DGNSS) techniques to retrieve inter-agent distances which can be in turn integrated to improve positioning performance. This article investigates an improved Bayesian estimation algorithm for a sensorless, tight-integration of DGNSS-based collaborative measurements through a modified Particle Filter (PF), namely Cognitive PF. Differently from Extended Kalman Filter and Unscented Kalman Filter indeed, a PF natively support the non-Gaussian noise distribution which characterizes DGNSS-based inter-agent distances. The proposed Cognitive PF is hence designed, implemented and optimized according to the architecture of a proprietary Inertial Navigation System (INS)-free Global Navigation Satellite System (GNSS) software receiver. Experimental tests performed through realistic radio-frequency GNSS signals showed a remarkable improvement in positioning accuracy w.r.t. reference PF and EKF architectures.

INDEX TERMS Bayesian estimation, global navigation satellite system, state estimation, particle filters, precise positioning, satellite navigation systems.

I. INTRODUCTION

Global Navigation Satellite Systems (GNSSs) are exploited nowadays in a wide range of applications with the aim of providing positioning and navigation capabilities to a growing number of devices [1], [2]. In parallel, Direct Short Range Communication (DSRC) and Ultra-Reliable Low-Latency Communication (URLLC) (e.g. 5G NR [3]–[5]) have disclosed possible near-real time exchange of data among neighbour vehicles such as position, velocity and heading [6], [7]. The combination of positioning capabilities along with the availability of raw measurements in high-end and mass-market devices [8]–[10], the auxiliary contextual measurements about the surrounding environment and the aforementioned modern communication channels has opened a variety of possibilities for navigation in harsh conditions. Among these, for example, vehicles can

periodically broadcast messages to other vehicles which can benefit from them in a plethora of manners. In particular, position information and auxiliary range data can be used, under certain conditions, to assess or refine the quality of the GNSS positioning solutions in a cooperative fashion [11], [12]. Ranging associated to the position estimate of a set of users actually provides opportunistic, additional landmarks to the positioning problem faced by conventional GNSS receivers. Therefore, in the last decades Collaborative Positioning (CP) has constituted a relevant topic in robotics, starting from a set of pioneering research works [13]–[15] up to recent paradigms integrating GNSS, proprioceptive and exteroceptive sensors [16], [17]. Several recent studies on CP have been focused on ranging sensors and technologies such as Ultra-Wide Band (UWB), LiDAR, ultrasound [18], [19], while few relevant literature contributions approached inter-vehicular range estimation through Differential GNSS (DGNSS) methods [20]–[24]. The latter is expected to bring information about the positioning problem according to the

The associate editor coordinating the review of this manuscript and approving it for publication was Zheng H. Zhu^{ID}.

statistics of the noise carried by the set of input measurements and to the relative spatial geometry of the involved receivers [11], [25]. A non-negligible amount of research contributions proposes integration schemes to fuse GNSS and auxiliary measurements obtained by independent ranging sensors. The errors affecting such measurements are often modelled as stationary additive contributions. However, when DGNS-CP is considered, a tight link between the relative dynamics of the receivers and the collaborative measurements computed via DGNS is responsible for non-negligible, non-stationary behaviours.

Monte Carlo Bayesian filters are generally known as optimal statistical tools to combine measurements from heterogeneous sources in order to enhance positioning performance [26], [27]. Despite of the non-linearity of the positioning problem (i.e. quadrilateration in GNSS), many solutions approach it by means of linearization (i.e. Weighted Least Square (WLS), Hybrid Extended Kalman Filter (EKF)). This methods also approximate generic probability distributions of the input measurements through Gaussian distributions, for practical reasons. In particular, when high accuracy is pursued, such mismodelled errors can induce a meter-level reduction in the accuracy of the solution. By considering pseudorange measurements affected by additive Gaussian-distributed noise, inter-agent distances (a.k.a. inter-receiver distances) computed by means of DGNS techniques mostly show non-Gaussian noise distribution. This turned conventional filtering approaches, such as the EKF, poorly effective [28] to reach meter-level accuracy through GNSS code-based measurements.

Early contributions exploited simpler schemes for the integration of auxiliary DGNS measurements, such as Maximum Likelihood (ML) and EKF by assessing the improvement on a simulation base only. The purpose of this work is instead the analysis of a statistics-adaptive sequential Bayesian estimation filter, namely cognitive Particle Filter (PF), suitable for such a class of non-stationary collaborative measurements. The study supports innovative receivers architectures conceived for *distance-based*, *distributed*, *sequential* and *probabilistic* positioning estimation, according to the taxonomy presented in [29]. The results achieved in this article were hence obtained by improving a modified PF [30]. The advantages of this sequential Bayesian estimation technique motivated the integration of GNSS-only auxiliary ranging measurements with the GNSS pseudorange measurements to achieve enhanced positioning accuracy. Among the Bayesian filters indeed, PF has the capability to natively handle non-Gaussian and non-linear measurement models [31], [32], thus, being properly tailored to the aforementioned measurements tight integration for positioning and navigation [27], [33], [34].

Despite of a higher computational complexity w.r.t. EKF and Unscented Kalman Filter (UKF), the PF has been considered in several applications related to GNSS. As far as the positioning problem is concerned, examples of low-cost advanced schemes were proposed in [35]–[37] for the

integration of Inertial Navigation Sytem (INS) and GNSS. Alternative techniques such as Adaptive Kalman Filter (AKF) and Strong Tracking Filter (STF) were proposed in literature to integrate different navigation systems [38] as well as federated solutions including hybrid filtering strategies. Recent contributions further explored the use of PF for different GNSS-based applications such multipath detection and mitigation [39].

The proposed study aim at supporting Network Localization and Navigation (NLN) which has been formalized from a theoretical perspective in several contributions [40]–[42]. According to the nomenclature proposed in [42], the investigated scenario addresses the Bayesian estimation performed through spatio-temporal cooperation among the receivers. However, the theoretical framework presented in [42] mostly addresses non-Bayesian methods. Non-Bayesian tight integration schemes have been extensively investigated in [11], [43] while the results presented in this article are specifically focused on the advances in the integration of correlated range measurements in Bayesian estimation based on PF. Within this paradigm inter-agent measurements are used and intra-agent quantities are estimated according to the evolution of the motion of the receivers. The proposed differential measurements cannot be treated indeed as regular independent distance measurements, and the strong covariance cross correlation of each range is responsible for the non-stationary behaviour of the quantities.

The paper outline is organized as follows: Section II recalls the fundamentals about DGNS ranging and Bayesian filtering applied to GNSS through PF. Section III introduces the optimizations proposed to improve positioning estimation accuracy and Section IV discusses the simulation setup exploited for the assessment. Section V discusses the improvement provided by the proposed approach to the paradigm of DGNS-CP and VI summarizes the main achievement of this study and the proposed further research goals.

II. METHODOLOGY

A. DGNS-BASED RANGING

The aim of any ranging technique is to provide an estimation of the distance between a reference location and a *target*, at a given time instant t_k , referred hereafter by means of the index k . Such a distance can be formally seen as the Euclidean norm of a displacement vector between two positions $\mathbf{x}_{a,k} = [x_{a,k} \ y_{a,k} \ z_{a,k}]$ and $\mathbf{x}_{b,k} = [x_{b,k} \ y_{b,k} \ z_{b,k}]$

$$\begin{aligned} d_{ab,k} &= \|\mathbf{d}_{ab,k}\| = \|\mathbf{x}_{a,k} - \mathbf{x}_{b,k}\| \\ &= \sqrt{(x_{a,k} - x_{b,k})^2 + (y_{a,k} - y_{b,k})^2 + (z_{a,k} - z_{b,k})^2}. \end{aligned} \quad (1)$$

The terms $\mathbf{d}_{ab,k}$ and $d_{ab,k}$ in (1) are also referred to as *baseline* and *baseline vector* in geodesy and DGNS applications. An estimation of $\mathbf{d}_{ab,k}$, thus of $d_{ab,k}$, can be obtained through the combination of sets of GNSS *raw observables* shared among networked GNSS receivers. Once the time

offset between two sets of measurements is compensated, DGNSS algorithms can be used to determine their inter-agent distance, as detailed in [2], [30]. The synchronization of multi-receiver measurements is out of the scope of this article but consolidated strategies addressed Doppler-based linear regression to cope for the misalignment among the measurements dumping epochs of different receivers [44], [45]. Assuming the receiver *a* as the *target agent* of this analysis, we consider that the *observable measurements* provided by the receiver *b* are synchronous to the GNSS timescale, thus they can be aligned to the measurements dumped by *a* at time instant t_k , referred to the same timescale. Whenever two generic GNSS satellites *r* and *s* are visible to both the receivers and the two pairs of measurements can be shared and synchronized as recalled above, a Double Difference (DD) measurement can be obtained as the difference of two Single Differences (SD)s between their pseudorange measurements

$$D_{ab,k}^{sr} = S_{ab,k}^s - S_{ab,k}^r = \Delta R_{ab,k}^{sr} + \varepsilon_{ab,k}^{sr} \quad (2)$$

where $S_{ab,k}^s$ is a single difference computed as $S_{ab,k}^s = \rho_{a,k}^s - \rho_{b,k}^s$, while $\varepsilon_{ab,k}^{sr}$ is a random variable collecting residual uncorrelated error contributions such as residual multipath, second-order noise components of the receiver front-ends and additional non-modelled noise contributions [46]. Such a quantity is often referred to as *aggregate error term* of the Double Differences (DD) measurement and is formally defined as

$$\varepsilon_{ab,k}^{sr} = \varepsilon_a^s - \varepsilon_b^r \quad (3)$$

where the right terms are the uncorrelated residual noise components observed by the receivers w.r.t. the *s*-th and *r*-th satellites, respectively. Figure 1 shows a pictorial representation of DGNSS-based ranging between a pair of receivers sharing measurements related to four visible GNSS satellites. In the bottom of the scheme, the horizontal position estimates are depicted along with their uncertainties, showed as error ellipses. By neglecting the aggregated error terms $\varepsilon_{ab,k}^{sr}$, the term $\Delta R_{ab,k}^{sr}$ can be expressed by highlighting the dependency from the *baseline vector* as

$$\Delta R_{ab,k}^{sr} = [\mathbf{h}_{a,k}^s - \mathbf{h}_{a,k}^r]^T \mathbf{d}_{ab,k} \quad (4)$$

where the generic \mathbf{h}^s is a *unitary steering vector* defined through the displacement vector between satellite and receiver estimated positions [46]. The computation of DD measurements can be obtained from the linear relationship $\mathbf{D}_{ab,k} = \mathbf{L}_{DD} \mathbf{S}_{ab,k}$, as

$$\underbrace{\begin{bmatrix} D_{ab,k}^{12} \\ D_{ab,k}^{13} \\ \vdots \\ D_{ab,k}^{1S} \end{bmatrix}}_{\mathbf{D}_{ab,k}} = \underbrace{\begin{bmatrix} -1 & 1 & 0 & \dots & 0 \\ -1 & 0 & 1 & \ddots & 0 \\ \vdots & \vdots & \ddots & \ddots & \vdots \\ -1 & 0 & \dots & \dots & 1 \end{bmatrix}}_{\mathbf{L}_{DD}} \underbrace{\begin{bmatrix} S_{ab,k}^1 \\ S_{ab,k}^2 \\ S_{ab,k}^3 \\ \vdots \\ S_{ab,k}^S \end{bmatrix}}_{\mathbf{S}_{ab,k}} \quad (5)$$

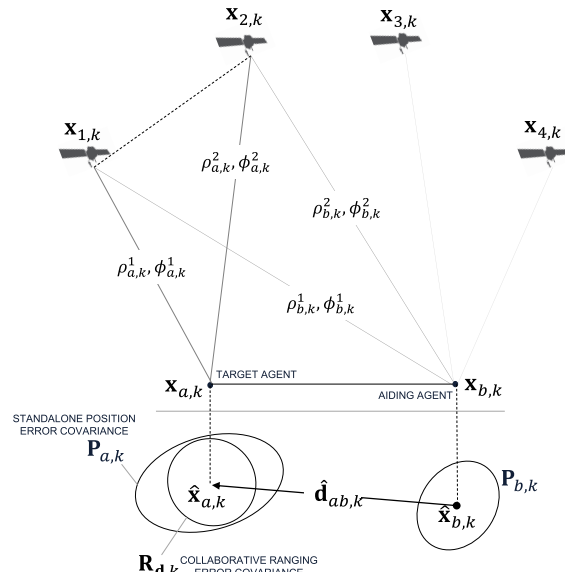


FIGURE 1. DGNSS ranging applied between two GNSS receivers sharing the measurements of four GNSS satellites. The dashed line represents the combination of single differences obtained w.r.t. the generic satellites $s = 1, q = 2$. Error covariances are depicted in form of error ellipses for the positioning solution and the baseline vector.

Equation (4) can then be expanded, neglecting the noise contribution in (2), as

$$\begin{bmatrix} D_{ab,k}^{12} \\ D_{ab,k}^{13} \\ \dots \\ D_{ab,k}^{1S} \end{bmatrix} \simeq \begin{bmatrix} \mathbf{h}_{a,k}^2 - \mathbf{h}_{b,k}^1 \\ \mathbf{h}_{a,k}^3 - \mathbf{h}_{b,k}^1 \\ \dots \\ \mathbf{h}_{a,k}^S - \mathbf{h}_{b,k}^1 \end{bmatrix} \mathbf{d}_{ab,k} \quad (6)$$

by collecting $S - 1$ double difference measurements from a set of S satellites simultaneously visible to *a* and *b*. A proper selection of the *reference satellite* typically leads to a better estimation. Given the *reference satellite* identified in (6) and (5) by apex 1, if $\varepsilon_{ab,k}^1 = \varepsilon_a^1 - \varepsilon_b^1$ can be considered negligible, then the error on the double differences can be approximated by the error of each single difference. Assuming independent and zero-mean random variables for ε_a^1 and ε_b^1 , the previous equality holds only if the standard deviations of both ε_a^1 and ε_b^1 are kept small. Therefore, the chosen *reference satellite* is expected to have high C/N_o values to both the GNSS receivers *a* and *b*. By denoting Φ_a^1 and Φ_b^1 as the C/N_o values from the reference satellite to receivers *a* and *b*, it is required that $\Phi_a^1 \geq \Phi_{Th}$ and $\Phi_b^1 \geq \Phi_{Th}$, where Φ_{Th} is the threshold. If more than one satellite satisfies this condition, the reference can be randomly selected among them. On the contrary, if no satellites satisfy the condition, the computation is discouraged.

By considering an effective selection of the *reference satellite*, the set of equations indicated in (6) can be solved to estimate $\mathbf{d}_{ab,k}$ through a WLS algorithm in the form

$$\hat{\mathbf{d}}_{ab,k} \simeq (\mathbf{H}_{D,k}^T \mathbf{H}_{D,k})^{-1} \mathbf{H}_{D,k}^T \mathbf{D}_{ab,k} \quad (7)$$

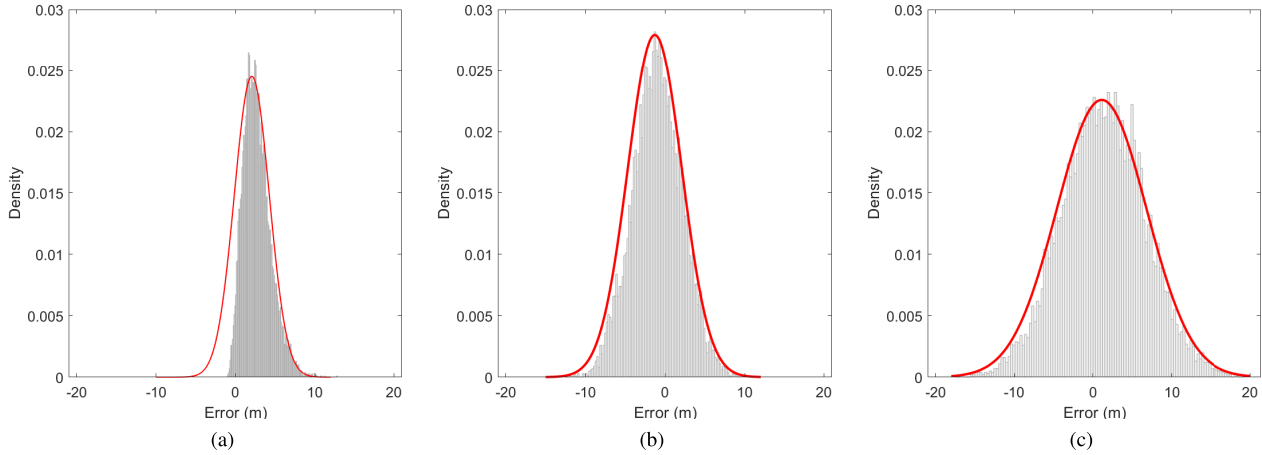


FIGURE 2. Experimental distributions of the inter-agent distance estimation error w.r.t. three independent, collaborative agents, compared to the corresponding Gaussian distributions (red curve) having the same mean and variance of the true distributions.

where $\mathbf{D}_{ab,k}$ and $\mathbf{H}_{D,k}$ are the first and the second term in (6), respectively. As for the other DGNS methods [47], uncorrelated errors such as different multipath reflections, can be increased by differentiation. Furthermore, according to [45], statistical assumption of mutual independence can be reasonable on different pseudorange measurements but it cannot be assessed for the resulting DD estimation. If the covariance matrix of the pseudorange measurements can be estimated by the receiver, it is possible to implement a weighted strategy to improve the accuracy of the baseline estimation. A general algebraic equation can be hence used to evaluate the covariance of the inter-agent collaborative measurements relying on the covariance of the WLS estimator in (7). It is then sufficient to compute

$$\mathbf{R}_{\mathbf{d},k}^{(DD)} = \left(\mathbf{H}_{D,k}^T \mathbf{H}_{D,k} \right)^{-1} \mathbf{H}_{D,k}^T \mathbf{R}_{DD,k} \mathbf{H}_{D,k} \left(\mathbf{H}_{D,k}^T \mathbf{H}_{D,k} \right)^{-1} \quad (8)$$

where \mathbf{R}_{DD} is the covariance matrix of the vector $\mathbf{D}_{ab,k}$ which is in turn computed from the SD covariance, as

$$\mathbf{R}_{DD,k} = \mathbf{L}_{DD,k} \mathbf{R}_{SD,k} \mathbf{L}_{DD,k}^T \quad (9)$$

where \mathbf{L}_{DD} is the linear relationship between SD and DD measurements, whose errors are still assumed independent for the two receivers. The use of a reference satellite for the construction of the DD implies that \mathbf{R}_{DD} is non-diagonal since the cross-correlation terms among these measurements cannot be neglected.

Therefore, a different method suitable to improve the accuracy of the estimation is foreseen in this study. A WLS-DD ranging technique is hence recalled hereafter. Assuming a non-equal variance of each ε^i , the weighted least squares estimator, i.e.

$$\mathbf{d}_{ab,k} = \left(\mathbf{H}_{D,k}^T \mathbf{W} \mathbf{H}_{D,k} \right)^{-1} \mathbf{H}_{D,k}^T \mathbf{W} \mathbf{D}_{ab,k} \quad (10)$$

can be implemented as the Best Linear Unbiased Estimator (BLUE), where $\mathbf{W} = \mathbf{R}_{DD}^{-1}$, is the *weight matrix* corresponding to the inverse of the covariance matrix of the double

difference vector, $\mathbf{D}_{ab,k}$. A simplistic evaluation of the *weight matrix* can be performed as follows. The noise contribution related to each single difference is assumed to be uncorrelated, so that \mathbf{W} can be simplified as

$$\mathbf{W} = \text{diag} \left(\frac{1}{(\sigma^1)^2}, \dots, \frac{1}{(\sigma^n)^2} \right) \quad (11)$$

where $\text{diag}(\cdot)$ denotes a diagonal matrix and σ^i is the standard deviation of ε^i . However, σ^i cannot be directly measured, unlike Φ_a^i and Φ_b^i . Therefore, assuming the noise is reversely proportional to the C/N_o , the variance can be expressed as

$$(\sigma^i)^2 \propto \frac{1}{(\Phi_a^i)^2} + \frac{1}{(\Phi_b^i)^2} \quad (12)$$

Sub-sequentially, the *weight matrix* \mathbf{W} is obtained by

$$\mathbf{W} = \text{diag} \left(\frac{(\Phi_a^1)^2 \cdot (\Phi_b^1)^2}{(\Phi_a^1)^2 + (\Phi_b^1)^2}, \dots, \frac{(\Phi_a^n)^2 \cdot (\Phi_b^n)^2}{(\Phi_a^n)^2 + (\Phi_b^n)^2} \right) \quad (13)$$

A further aspect must be considered: the *selection of the candidate satellites*. The DD ranging can be applied only when at least four satellites are visible to the two receivers. Therefore, in addition to the *reference satellite*, at least other three candidate satellites have to be selected. First of all, a minimum threshold ϕ_{min} is set to prevent the use of pseudorange measurements providing highly noisy measurements. Thus, only the satellites with C/N_0 values higher than ϕ_{min} can be selected. If the number of candidate satellites is less than three, computation is not performed. It has to be noticed that $\phi_{min} \leq \phi_{ref}$ generally holds, since the reference satellite is expected to have the highest C/N_0 value. To the aim of this study, it is worth noticing that the output of the proposed WLS-DD shows different statistical behaviour according to the relative position of the collaborating users. As shown in the example of Figure 2 indeed, the auxiliary inter-agent distances computed at the same time instant through different sets of shared pseudorange measurements exhibited non-Gaussian and non-stationary behaviours.

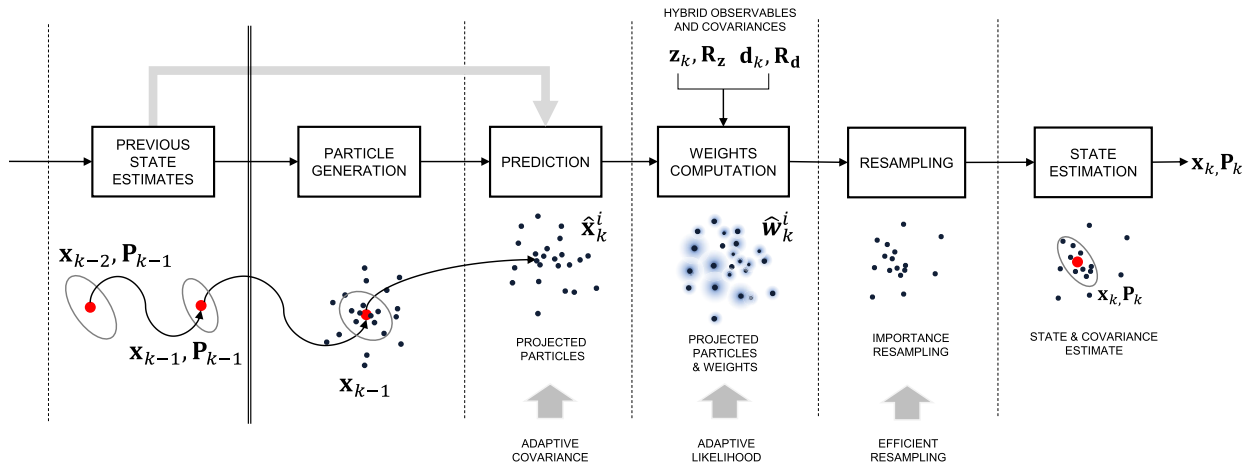


FIGURE 3. Conventional processing stages of a PF and hybridized input measurements for the tight integration of DGNSS inter-agent distances (grey arrows indicate the optimizations proposed in the study).

B. DGNSS-BASED COLLABORATIVE POSITIONING THROUGH BAYESIAN ESTIMATION

Earlier contributions showed the considerable benefits of integrating DGNSS-based inter-agent distances in GNSS-only positioning and navigation. Furthermore, collaborative Bayesian estimation demonstrated superior performance w.r.t. to the standalone GNSS positioning at the cost of a negligible additional complexity and a pre-existing network infrastructure. It is worth remarking that high-end receivers usually include multiple network interfaces and the mass-market receivers are typically embedded in mobile networked devices, thus being natively enabled to data sharing.

The tight-integration schemes of DGNSS measurements relying on EKF and suboptimal PF were described and discussed in detail in [44] and [30], respectively. For the sake of completeness, the general architecture of the PF is briefly recalled hereafter. The Monte Carlo Bayesian estimation foreseen by the use of PF is based on the processing of a set of particle, according to the workflow reported in Figure 3. Compared to other Bayesian filters, thanks to the Monte Carlo approach the PF has the capability to natively handle non-Gaussian and non-linear measurement models. In general, PF provides a better solution dealing with scenarios where Kalman Filter (KF)-based methods diverge due to linearization and approximation operations. The drawback is an increment of the computational complexity with respect to the EKF, as the number of particles increases [30], [48]. A hybrid Position Time Velocity (PVT) computation model based on PF can be provided by integrating the set of auxiliary ranging measurements, \mathbf{d}_k , with conventional GNSS pseudorange and Doppler measurements, \mathbf{z}_k and optimizing the PF for navigation purposes.

The set of particles is generated over a region according to a given statistical distribution:

$$\hat{\mathbf{x}}_k^i \sim \mathcal{D}(\mathbf{x}_{k-1}, \mathbf{P}_k) \tag{14}$$

where the index i identifies the i -th particle, \mathbf{x}_{k-1} is the previous state estimate, \mathbf{P}_k is the state covariance matrix and \mathcal{D} represents a generic statistical distributions (e.g. Gaussian, Rayleigh). A particle $\hat{\mathbf{x}}_k^i$ represents a possible realization of the receiver state vector at time t_k , defined as

$$\hat{\mathbf{x}}_k^i = [x_k^i \ y_k^i \ z_k^i \ b_k^i \ \dot{x}_k^i \ \dot{y}_k^i \ \dot{z}_k^i \ \dot{b}_k^i] \tag{15}$$

where $[x_k^i \ y_k^i \ z_k^i]$ refers to the spatial coordinates, $[\dot{x}_k^i \ \dot{y}_k^i \ \dot{z}_k^i]$ to the axial velocity components, while b_k^i and \dot{b}_k^i are respectively the bias and the drift of the local clock. After each particle $\hat{\mathbf{x}}_k^i$ is predicted following the dynamic system model, the nominal measurement vector $\hat{\mathbf{z}}_k^i$ is computed. At this point, the auxiliary ranges are integrated by appending them to $\hat{\mathbf{z}}_k^i$, creating a new nominal measurements vector $\bar{\mathbf{z}}_k^i$ as

$$\bar{\mathbf{z}}_k^i = [\mathbf{z}_k^i \ \mathbf{d}_k^i]. \tag{16}$$

The weights are then obtained by relying on a pre-defined Probability Density Function (PDF) model, $p(\mathbf{z}_k | \hat{\mathbf{x}}_k^i)$, by estimating the likelihood $\mathcal{L}(\bar{\mathbf{z}}_k | \hat{\mathbf{x}}_k^i)$ w.r.t. the expected measurements computed for each particle $\hat{\mathbf{x}}_k^i$. The weights are hence computed as

$$w_k^i = \frac{\mathcal{L}(\bar{\mathbf{z}}_k | \hat{\mathbf{x}}_k^i)}{\sum_{i=1}^N \mathcal{L}(\bar{\mathbf{z}}_k | \hat{\mathbf{x}}_k^i)} = \frac{\prod_i p(z_{n,k} - z_{n,k}^i)}{\sum_{i=1}^N \prod_i p(z_{n,k} - z_{n,k}^i)}. \tag{17}$$

A number of resampling methods can be used to redistribute the set of particles and accurately model any generic PDF of the state vector (e.g. multivariate distributions) [34].

As an example, the *Bayesian bootstrap* foresees the selection of N samples from the particle set $\{\mathbf{x}_k^i\}$ with a picking probability w_k^i . When a uniform distribution is used to determine the picking probability $w_k^i = 1/N$, the method is also referred to Sampling Importance Resampling (SIR). An alternative strategy is named *Importance Sampling* and it foresees the re-sampling according to the Bayesian bootstrap only if the number of samples is lower than a *resampling threshold*

$$N_\theta = \frac{1}{\sum_i (w_k^i)^2} < N_{th} \quad (18)$$

provided that the number of effective particles $1 \leq N_\theta \leq N$.

The state estimation is eventually given by the weighted average of the generated particles.

Given a sufficient number of generated particles, the covariance matrix \mathbf{P}_k associated to the state estimate \mathbf{x}_k , can be numerically estimated through the *sample covariance* computable over the set of the output particles, \mathbf{x}_k^i .

C. ASSUMPTIONS AND PRELIMINARY FINDINGS

A set of assumptions related to the cooperative framework and the use of PF-based Bayesian estimation are summarized hereafter.

1) ERROR PROPAGATION

Trusted position estimates and measurements are assumed to be exchanged among cooperative receivers. Intuitively, any bias affecting the state estimates of the aiding agent b , used as an anchor, negatively affects the estimation of the state estimate of receiver a . However, when unbalanced conditions are experienced by receivers a and b and the aiding agent can rely on higher precision and accuracy of its estimates, a pairwise cooperation could considerably improve the performance of the aided/target agent, as depicted in Figure 4. The position uncertainty of the *aiding receiver* must be considered in the form of its position error covariance, $\mathbf{P}_{b,k}$. While the error covariance of the inter-agent distance, $\mathbf{R}_{d,k}$, models the error on the ranging only, $\mathbf{P}_{b,k}$ must be taken into account when such measurement is integrated by relying on the position of the receiver b . By assuming independent noise distribution on the input measurements, the error covariance $\mathbf{P}_{b,k}$ can be summed to the covariance of the baseline length, $\mathbf{R}_{d,k}$ to provide a more accurate error model, leading to $\mathbf{R}_{d,k}^*$. According to this model, possible aiding receivers experiencing high uncertainty are weighted accordingly and they can be neglected among all the available anchors in a multi-receivers scenario.

2) INFORMATION COUPLING

Since the estimated position at time instant t_{k-1} is exploited for the estimation of the state vector at the current instant t_k , the *information coupling* among the state vectors of the cooperating receivers cannot be avoided. However, despite of the link between the receivers state estimates from the first cooperation instant on, the discussed GNSS-based

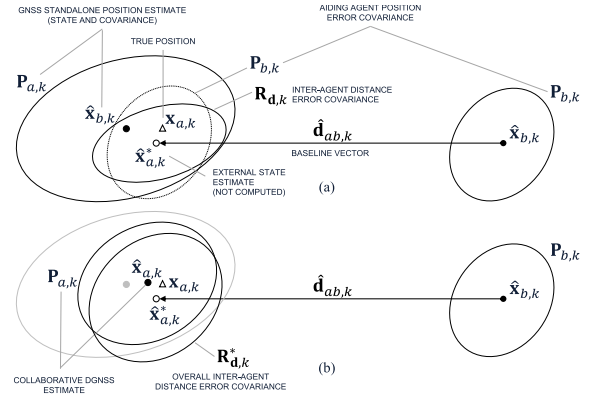


FIGURE 4. 2D propagation of the position uncertainty of the *aiding receiver, b*, from a collaborative inter-agent distance (a) to the collaborative state estimation of the *aided agent (b)*. Error covariances are depicted in form of error ellipses.

framework coupled with the modified PF with the following optimization steps allows to assume a reasonable independence between the positioning solutions. By treating the information obtained as a-priori information of the receiver state at t_{k-1} , and obtained as the product of intra-receiver measurement, each cooperative state estimation is assumed independent.

3) PERFORMANCE

In order to compare the benefits of the PF w.r.t. to more popular EKF, a suboptimal PF architecture was proposed in [30]. As shown in Figure 5 that implementation offered unsatisfactory performance on the investigated scenario, thus motivating further research effort towards the optimization of a subset of stages composing the PF workflow (highlighted by the bottom-up arrows in Figure 3). Unsatisfactory performance in accuracy was initially observed in the proposed scenario. A set of reference values are summarized in Table 1 for different percentiles. Indeed, such a performance was mostly attributed to a suboptimal processing of the inter-agent distances.

TABLE 1. Improvement in the positioning accuracy provided through single collaborative contributions from independent aiding receivers, assuming a Gaussian model for the auxiliary measurement retrieved along a rectilinear trajectory. Percentiles are indicated by PCTL.

Aiding Peer	50-th PCTL Improv. (%)	75-th PCTL Improv. (%)	95-th PCTL Improv. (%)
Agent #1	14.07	1.89	2.31
Agent #2	2.35	-0.24	-3.92
Agent #3	10.17	-6.6	6.90
Agent #4	-2.60	-8.64	-1.9

III. PROPOSED OPTIMIZATION

Prior to consider a cooperative scenario, the implemented PF was optimized by focusing on the *particle generation* process and the *resampling* procedure. The first was intended

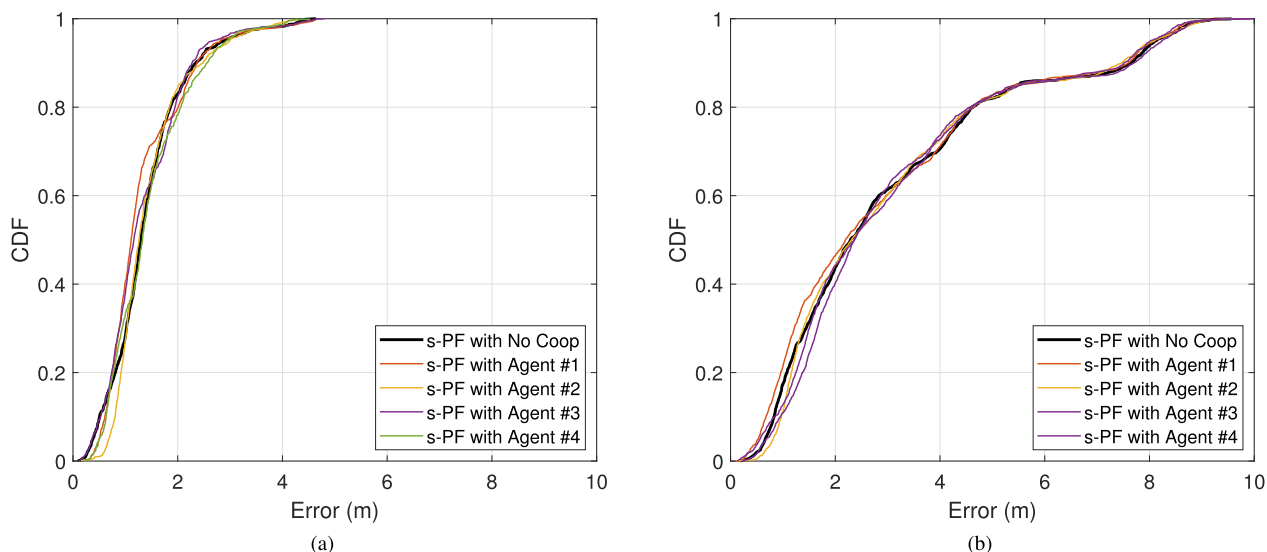


FIGURE 5. Examples of ECDFs of the position error for the suboptimal implementation of a PF tightly integrating single collaborative DGNSS measurements on a rectilinear trajectory (a) and on a complex scenario (b), w.r.t. independent aiding receivers.

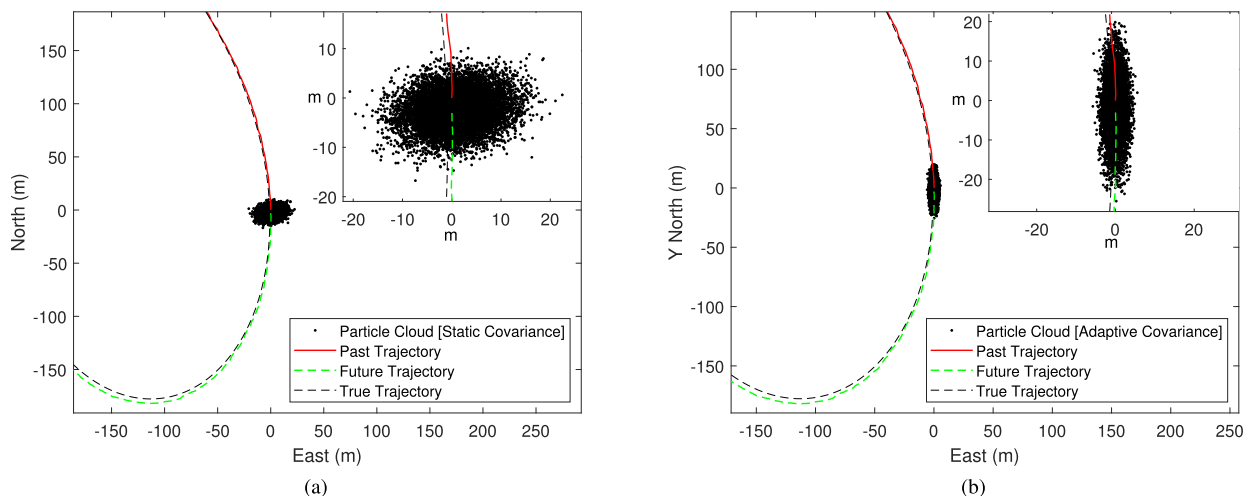


FIGURE 6. Effect of conventional (a) and adaptive (b) covariance matrix on particles generation.

to cope with the lack of additional data usually provided by INSS, but not available in the investigated receiver architecture. The latter was instead pursued to reduce the computational complexity of the simulation environment thus making the proposed scheme more appealing for practical implementation in mass-market electronics.

A. INITIALIZATION: ADAPTIVE COVARIANCE

To emulate the additional information typically provided by proprioceptive sensors such as INSS, a memory is introduced in the estimation process concerning the evolution of the motion along the time. An adaptive method was hence proposed to reduce the waste of particles generated as unlikely states (i.e. physically infeasible velocity and location states). The proposed dynamic *position error covariance* was conceived to dynamically adapt the estimation to the state evolution of the system over time by exclusively relying on the

kinematics described by the previous fixes. At each time instant indeed, the *position error covariance* was computed by exploiting a set of previous position estimates (the last four were considered for the results presented in Section V) and it provided a measure of the variation of the position vector itself. Accordingly, the PF can generate the particle cloud by adapting it to the motion of the target at time instant t_k . A visual comparison is shown in Figure 6 in which the estimated covariance foreseen by conventional PF scheme has been replaced with the proposed adaptive covariance to achieve a better particle spreading according to the motion of the receiver.

B. UPDATE: ADAPTIVE LIKELIHOOD

To achieve an optimized PF implementation, the GNSS pseudoranges (and Doppler) measurements and the auxiliary inter-agent distances can be respectively processed

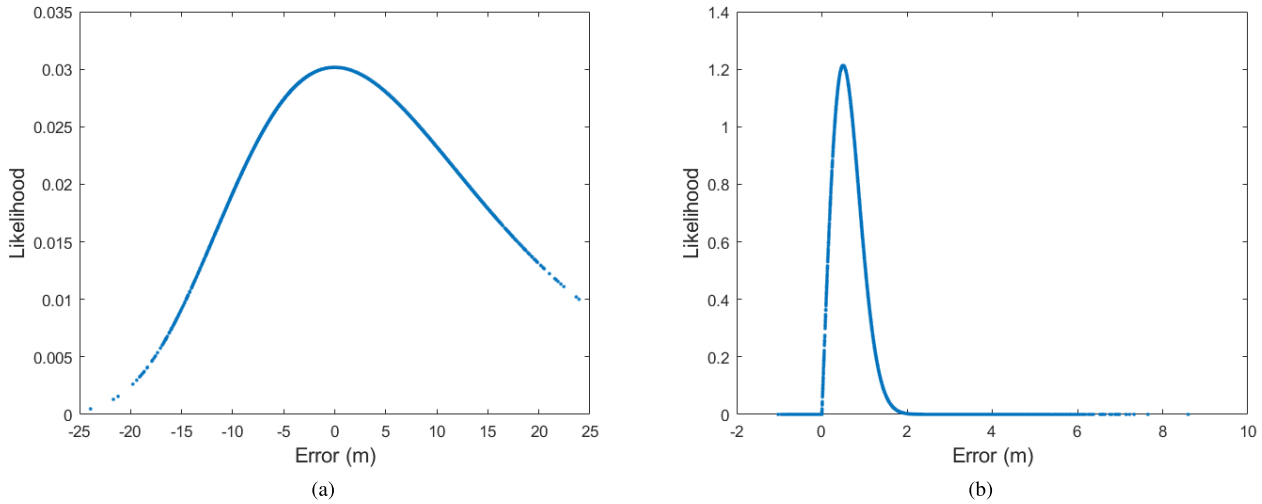


FIGURE 7. Examples of experimental GEV (a) and Rayleigh (b) PDFs exploited for the likelihood estimation in the proposed Cognitive PF architecture.

as Gaussian-distributed and non-Gaussian-distributed random quantities, by generating two different likelihood functions, as

$$p(\mathbf{z}_k | \hat{\mathbf{x}}_k^i) \sim \mathcal{N}(0, \mathbf{R}_z) \quad (19)$$

$$p(\mathbf{d}_k | \hat{\mathbf{x}}_k^i) \sim \mathcal{D}(0, \mathbf{R}_d) \quad (20)$$

where \mathbf{R}_z and \mathbf{R}_d are the so called *observation noise covariance* matrices and $\mathcal{D}(0, \mathbf{R}_d)$ is a generic non-Gaussian distribution. The two likelihoods were then used for the weight computation.

Preliminary investigations about the error distribution of DGNSS range measurements provided that WLS-DD range measurements can be reliably modelled through GEV or Rayleigh distributions when they are obtained from Gaussian-distributed input pseudoranges. Both of them depend on two *shape parameters* (k for GEV and σ for Rayleigh) which modify the shape of their PDF. When the two distribution models are integrated in the PF, these parameters affect the generation of the likelihood, thus the accuracy of the state estimation.

1) GEV AND RAYLEIGH DISTRIBUTIONS

The GEV distribution combines together the Gumbel, Fréchet and Weibull distributions into a single family to allow a continuous range of possible shapes. Its characteristic parameters are the *shape parameter* k , the *location parameter* μ and the *scale parameter* σ , and the distribution is classified as type I, II and III when $k = 0, k > 0$ and $k < 0$, respectively. Based on the extreme value theorem, the GEV distribution is the limit distribution of properly normalized maxima of a sequence of independent and identically distributed random variables [49], [50]. The PDF of the GEV distribution used in this study according to the aforementioned parameters is

$$f(x|k, \mu, \sigma) = \frac{1}{\sigma} e^{-(1+k\frac{x-\mu}{\sigma})^{-\frac{1}{k}}} (1+k\frac{x-\mu}{\sigma})^{-1-\frac{1}{k}} \quad (21)$$

for

$$1 + k\frac{x-\mu}{\sigma} > 0.$$

For $k = 0$ the PDF becomes

$$f(x|0, \mu, \sigma) = \frac{1}{\sigma} e^{-e^{-\frac{x-\mu}{\sigma}}} - \frac{x-\mu}{\sigma} \quad (22)$$

In Figure 7a, a generic GEV-shaped likelihood for $k = 0$ is shown.

Rayleigh distribution can also model the statistics of the inter-agent distances with a good accuracy and is defined as a continuous probability distribution for non-negative-valued random variables. Its PDF can be expressed as

$$f(x|\sigma) = \frac{x}{\sigma} e^{-\frac{x^2}{2\sigma^2}}. \quad (23)$$

In Figure 7b, a generic likelihood obtained by applying a Rayleigh Distribution with $\sigma = 0.5$ is shown. The optimized PF is conceived to perform the weight computation of the generated particles by dealing with two different likelihood families: likelihood functions based on Gaussian PDFs for the pseudoranges and likelihoods based on non-Gaussian PDFs for the DGNSS inter-agent distances.

C. EFFICIENT RESAMPLING

An effective resampling method is required to prevent high concentration of the probability mass on a few particles by ensuring in parallel reasonable computational complexity. Without resampling, after few iterations PF will collapse to a single particle with weight equal to 1, while all the other particles will have negligible weights [51]. This is the so called *degeneracy phenomenon*. The most popular resampling algorithm is defined as SIR. Other resampling algorithms, such as *stratified*, *residual* and *systematic* resampling may be applied as well. In terms of accuracy and precision performance, the difference among the resampling methods is negligible

being in the order of few centimetres, in particular by considering remarkable amounts of particles (i.e. 10^4). A comparison among the computational time (in single-threaded MATLAB[®] computation) of the four resampling methods is instead reported in Table 2.

TABLE 2. Comparison of the execution time of the investigated resampling methods. (MATLAB execution on single-threaded vectorized processing of the particles).

Resampling Algorithm	Execution time (s)
Sampling Importance	1196
Residual	115
Stratified	76
Systematic	68

From Table 2 indeed, it emerges how residual, stratified and systematic methods drastically reduce the execution time of the overall computation by a factor $10 \sim 15$ with respect to the popular SIR algorithm, in particular the *systematic* and *stratified* algorithms. The last one is preferable, due to the possibility to be implemented in a parallel architecture (e.g. Graphic Processing Unit (GPU)). The main principle of the *systematic* and *stratified* resampling algorithms is to set the number of generated particles, N , from the uniform distribution

$$u_i \sim \mathcal{U}[0, 1), \quad i = 1, \dots, N \quad (24)$$

and selecting particle $\hat{\mathbf{x}}_k^j$ for replication, if

$$u_i \in \left[\sum_{p=1}^{j-1} w^p, \sum_{p=1}^j w^p \right). \quad (25)$$

In particular, the *stratified resampling algorithm* works by considering a division into strata (layers) according to the number of particles. The resampling procedure is hence performed simultaneously within each of them. The algorithm, which can be easily implemented with complexity $O(N)$, assumes that the range $[0, 1)$ is subdivided into equal parts, and the draw occurs in each stratum

$$u_i \sim \mathcal{U} \left[\frac{i-1}{N}, \frac{i}{N} \right). \quad (26)$$

Particles $\hat{\mathbf{x}}_k^j$ are then selected for replication according to (25) [52]. Eventually, they are averaged to achieve the pursued state estimation, as recalled in the general filter workflow presented in Section II-B.

D. CONSIDERATIONS ON COMPUTATIONAL COMPLEXITY

The adaptive covariance estimation discussed in Section III-A, is performed once per PVT epoch. It does not depend on the number of particles N , hence it does not increase the computational complexity as well as it holds for the *adaptive likelihood*, presented in Section III-B. Indeed, the *adaptive likelihood* can be pursued by estimating the static behaviour of the inter-agent distances prior to their

integration in the navigation filter. Within actual implementations it can be performed in parallel by a dedicated algorithmic unit in charge of combining the heterogeneous measurements into collaborative distances. The likelihood functions used in the weight computation must be adjusted according to the behaviour of the differential quantities and of the experimental conditions (i.e. receivers and satellite geometry, non-stationary measurements noise).

IV. SIMULATION SETUP

An experimental setup inherited from the one presented in [30], was selected to analyse the performance of the optimized PF by dealing with realistic GNSS signals and dynamic Global Positioning System (GPS) satellite constellation. The other GNSSs constellations (i.e. Galileo, GLONASS, Beidou) are omitted without any loss of generality.

A. VEHICULAR SCENARIO

A vehicular scenario was first generated to extract the reference trajectory and the state vector of each simulated receiver with a position update rate of 10 Hz. The generated files were then processed through a Radio-Frequency Constellation Simulators (RFCS) IFEN[®] NavX. The GNSS signals were generated for a dynamic GPS constellation provided in Figure 8a. They were transmitted by the RFCS and hence digitalized by means of the Analog-to-Digital Converter (DAC) converter embedded in a Universal Software Radio Peripherals (USRP[™]) N210, disciplined in turn by a compact RFX-OS364 Oven-Controlled Crystal Oscillator (OCXO). The resulting output binary files (.bin) were then processed through a MATLAB[®]-based fully-software receiver (NavSAS Rx) to obtain raw GNSS observables out from the tracking stage and the epochs timestamps out from a preliminary PVT stage. A further MATLAB[®] script was used to combine auxiliary and local pseudorange measurements into collaborative inter-agent distances. In order to reduce the amount of time-consuming single-receiver simulations and with the aim of preserving a considerable variability of the observable processes, a Bernoullian path was designed as shown in Figure 8b. The Bernoullian trajectory was centered at a given reference location (45.067825° Latitude, 7.591147° Longitude), over an area of approximately 0.4 km^2 . A set of four receivers C_1, C_2, C_3 and C_4 was kept static while the target moved along the path according to the dynamics depicted in Figure 9a. The use of static collaborating receivers has not to be considered as a simplification of the scenario. Their static location indeed does not imply a lack of generality in terms of relative dynamics w.r.t. the GNSS satellites.

The true state vector of each receiver was generated through the MATLAB[®] Driving Scenario simulation environment and stored as .trj2 file to feed the RFCS for the generation of the trajectories. The snapshot in Figure 8b shows a possible

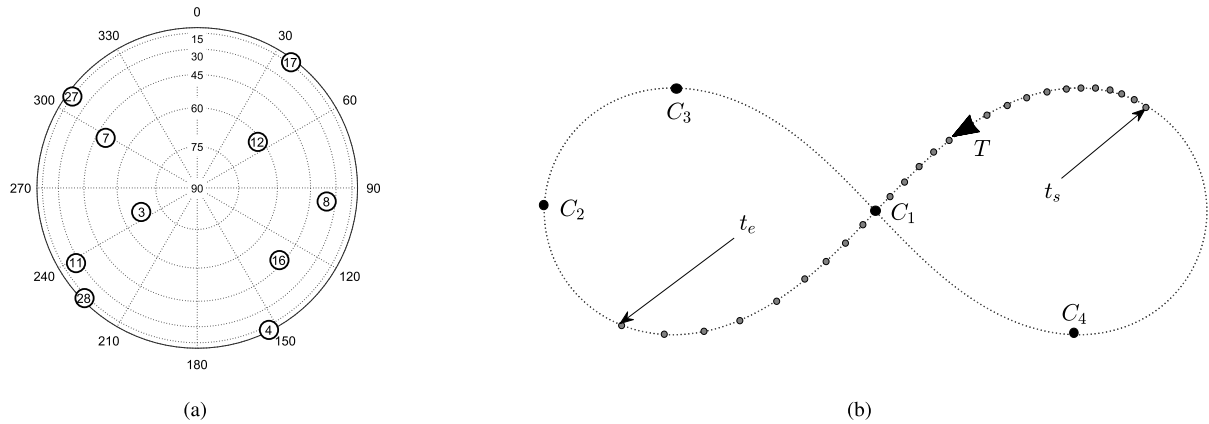


FIGURE 8. Snapshot of satellites positions on a skyplot (a) and of a simulated trajectory travelled by the target receiver T within the experimental setup.

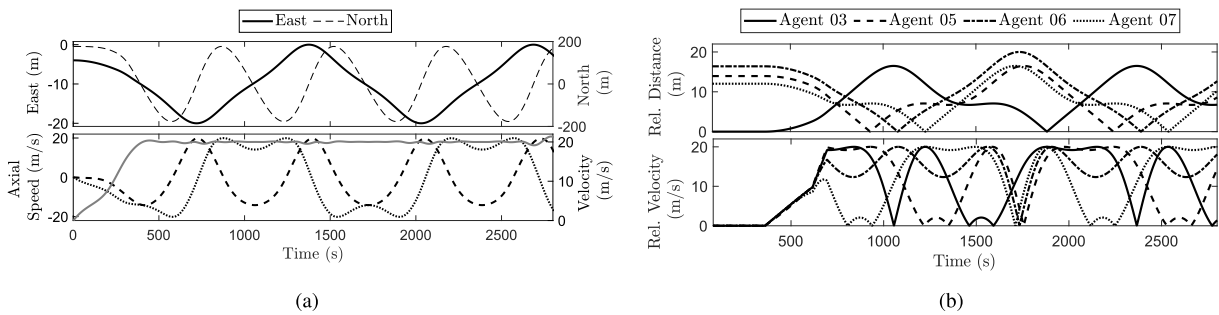


FIGURE 9. Simulated absolute dynamics of the target receiver (a) and simulated relative dynamics of a set of aiding receivers w.r.t. the target in East-North (EN) reference frame.

realization of the test in which the target receiver a can benefit from the collaboration of receiver C_1, C_2, C_3 and C_4 .

As shown in Figure 9a and Figure 9b, an evident periodicity is visible due to the multiple laps travelled on the Bernoullian lemniscate. Different timespans were selected to provide an exhaustive collection of output results. The integration of inter-agent distances was hence performed through the tight integration scheme mentioned in Section II, by compensating for the lack of GNSS measurements typical of urban environment. The geometry of the network must be certainly taken into account when considering the reliability of the receivers, since the accuracy of the relative positioning estimates depends strongly on the local position of the target with respect to the receivers at each time instant [11], [40]. After the preliminary optimization on the particle generation discussed in Section III, auxiliary inter-agent distances were integrated in the filter. A first set of results were obtained by considering a suboptimal implementation of the PF, which forces the non-Gaussian error distributed range measurements to match Gaussian likelihood model [30].

B. FILTER CONFIGURATION

According to the key parameters discussed in Section II-B and to the early findings presented in [30], the PF was initialized with the following values: number of particle,

$N = 10^4$; sampling threshold $N_{th} = 4000$. The number of particles is a tradeoff between computational complexity and the magnitude of the trace of the output state covariance. It is worth remarking that in this study a 8-states state vector was consider, as in (15). Despite of the relevance of the setup in terms of accuracy estimation, a comparison among different amounts of particles and resampling thresholds is out of the scope of this work. The values assigned to the configuration parameters have been chosen heuristically for the dataset under test according to the preliminary analysis in [30].

V. RESULTS

The section summarizes the improvement obtained by means of the proposed optimized stages discussed in Section III. Given that the *stratified resampling algorithm* has a negligible impact on the positioning accuracy, this section only includes the improvement provided by the implementation of *adaptive covariance* and *adaptive likelihood* characterizing the proposed cognitive PF.

A. ADAPTIVE COVARIANCE

A comparison between the cumulative density function of the positioning error, namely ECDF, obtained using conventional *state covariance matrix* and the proposed adaptive solution is shown in Figure 10.

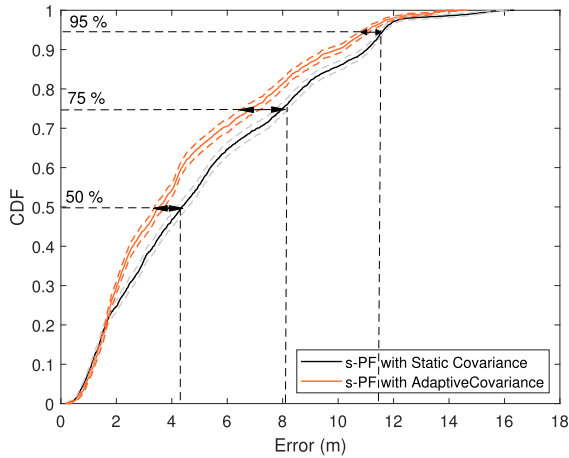


FIGURE 10. ECDFs of the position error comparing conventional and adaptive covariance model for particles generation (dashed red and grey curves show the 95% confidence interval).

An accuracy improvement of 20.02 % is achieved at the 50-th percentile, while a poorer although positive improvement can be observed at the higher percentiles, as shown in Table 3. As expected, the positioning accuracy was enhanced by making PF able to adapt the particle cloud shape to the current receiver kinematics, without feeding the filter with additional measurements as typically provided by INS. This solution is particularly effective to restrain tangent drifts along non-rectilinear portions of the trajectory [50].

TABLE 3. Evaluation of the position error for conventional and adaptive covariance model.

Covariance Model	50-th PCTL Error (m)	75-th PCTL Error (m)	95-th PCTL Error (m)
Conventional Model	4.34	8.03	11.84
Adaptive Model	3.47	6.76	10.90
Improvement (%)	20.02	15.78	7.91

B. STATISTICS-ADAPTIVE LIKELIHOODS

GEV and Rayleigh distribution models introduced in Section III are considered hereafter and an analysis of the positioning ECDF is presented in Figure 11 and Figure 15 by varying their shape parameters (k for GEV and σ for Rayleigh). After optimal k and σ values were identified, a comparison between the two models and the Gaussian distribution was performed by considering different portions of the trajectory and the related timespans. It is shown how GEV distribution for $k = \{0, 0.5, 1\}$ provides better accuracy w.r.t. the Gaussian distribution.

Table 4 and Table 5 show respectively the Root Mean Square Error (RMSE) of the positioning solution measured on a 180s and 300s timespans, respectively. It can be noticed that the estimation of GEV *shape parameter*, k , is of paramount importance to ensure higher positioning performance w.r.t. a generic Gaussian model, tailored on the covariance estimate for the current set of measurements. However,

TABLE 4. Evaluation of the position error for different PDF models of the inter-agent distances considering 180 s of PVT computation.

Distribution Model	50-th PCTL Error (m)	75-th PCTL Error (m)	95-th PCTL Error (m)
Gaussian Distr.	2.29	4.31	8.05
GEV Distr. [$k = 0$]	2.40	4.38	8.21
GEV Distr. [$k = 0.5$]	2.25	3.71	7.50
GEV Distr. [$k = 1$]	2.59	4.33	7.29
Rayleigh Distr. [$\sigma = 0$]	3.25	5.29	8.56

TABLE 5. Evaluation of the position error for different PDF models of the inter-agent distances considering 300 s of PVT computation.

Distribution Model	50-th PCTL Error (m)	75-th PCTL Error (m)	95-th PCTL Error (m)
Gaussian Distr.	3.50	6.98	11.04
GEV Distr. [$k = 0$]	3.66	7.21	11.18
GEV Distr. [$k = 0.5$]	3.19	6.13	9.78
GEV Distr. [$k = 1$]	3.64	5.90	9.21
Rayleigh Distr. [$\sigma = 0$]	4.18	7.57	12.02

the GEV distribution generally induces higher accuracy w.r.t. the Rayleigh counterpart. These results confirm that a Gaussian approximation is not optimal for the tight-integration of WLS-DD collaborative measurements.

However, the performance shown by the single GEV distributions obtained by varying the *shape parameter*, k , are quite different when different portions of the trajectory were considered. Thus, an adaptive implementation of the distribution for the likelihood function of the inter-agent distances is advisable according to the overall geometrical configuration of the receiver network, thus to the geometry of the aiding contributions.

To assess the potential of the proposed Cognitive PF navigation filter, the full trajectory was split into six sectors, as shown in Figure 13. For each sector, an estimate of the PDF of the the implemented collaborative contributions was performed to identify the matching likelihood functions in the *weight computation*. Eventually, the PVT computation was performed sector-by-sector and the distribution which provided the best target positioning accuracy along that sector was a-posteriori selected according to Table 6.

As we can qualitatively notice from the PDF histograms referred to each sector, Gaussian distribution fitting (red curves) could be still considered a valuable choice

TABLE 6. A-posteriori adaptive selection of the distribution models for the likelihood of the inter-agent distances.

Trajectory Sector	Selected Distribution Model
Sector 1	GEV Distr. [$k = 0$]
Sector 2	GEV Distr. [$k = 1$]
Sector 3	GEV Distr. [$k = 0.5$]
Sector 4	GEV Distr. [$k = 0$]
Sector 5	GEV Distr. [$k = 1$]
Sector 6	GEV Distr. [$k = 1$]

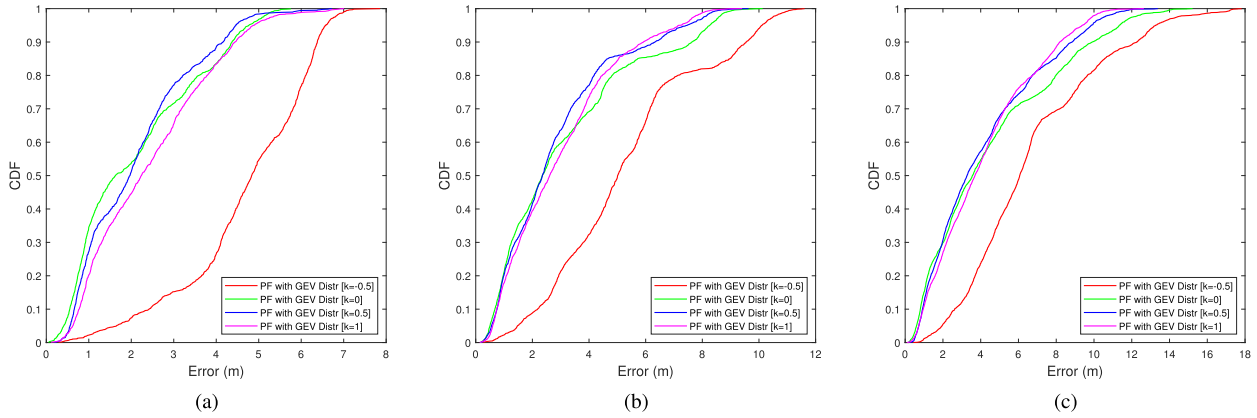


FIGURE 11. ECDF of the position error for a cognitive PF using GEV-distributed likelihood for the inter-agent distances, over 120 s (a), 180 s (b) and 300 s (c) of PVT computation.

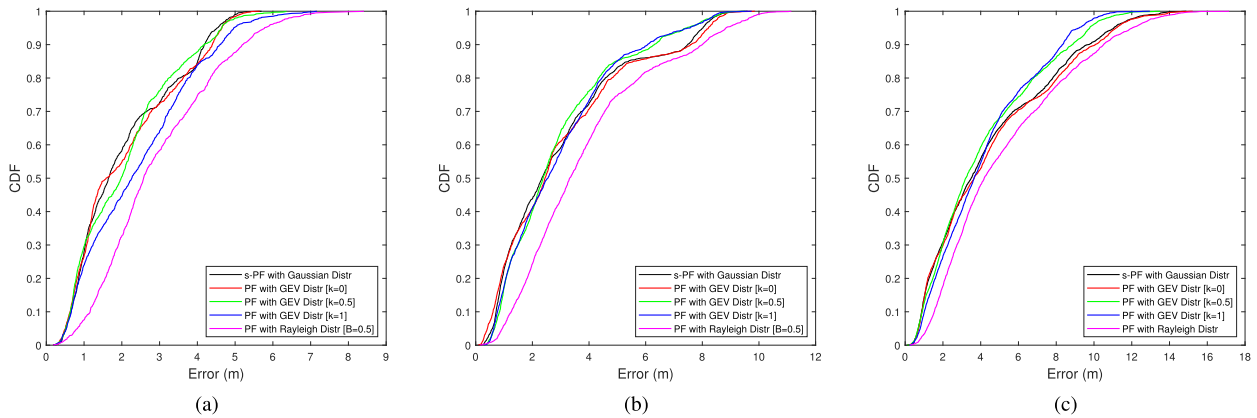


FIGURE 12. ECDFs of the position error comparing different distributions for inter-agent distances varying the shape parameter k , over 120 s (a), 180 s (b) and 300 s (c) of PVT computation.

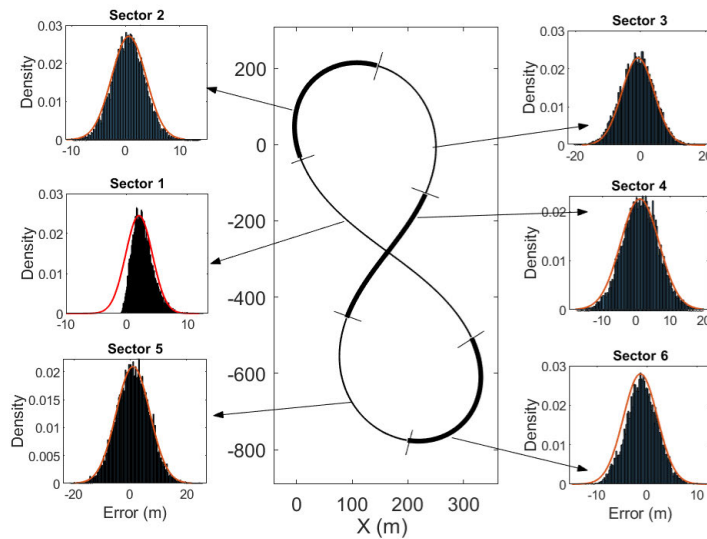


FIGURE 13. Sectorization of the trajectory traveled by the target agent according to the a-priori knowledge of the noise statistical distribution of the inter-agent distances computed w.r.t. the a single aiding agent.

since it appears well approximating the true PDFs. However, the following quantitative analysis clarified that the

non-stationarity of the distribution must be taken into account to ensure higher position accuracy.

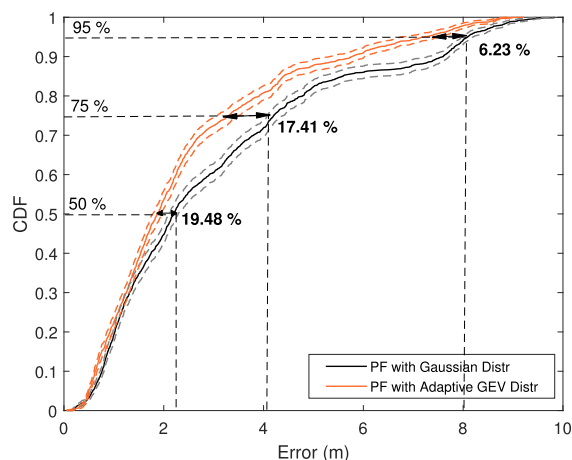


FIGURE 14. ECDF curve comparing the statistics of the position error obtained through a PF using adaptive GEV Distribution and a s-PF using Gaussian Distribution for the likelihood estimation of collaborative measurements (dashed lines show the 95% confidence interval).

TABLE 7. Position errors and improvement evaluation applying a-posteriori adaptive distribution model selection.

Distribution Model	50-th PCTL Error (m)	75-th PCTL Error (m)	95-th PCTL Error (m)
Gaussian Model	2.31	4.25	8.02
Adaptive GEV Model	1.86	3.51	7.52
Improvement (%)	19.48	17.41	6.23

The positioning solutions computed by adapting the likelihood of the collaborative contributions were indeed combined and an assessment simulation was performed by applying the optimal a-posteriori distribution for each sector. A comparison with the Gaussian distribution used in the early suboptimal implementation is presented in Figure 14. A quantitative comparison is presented in Table 7 which summarizes the position error (and the accuracy improvement) achieved by using a suboptimal stationary Gaussian model and the proposed statistics-adaptive GEV model. A remarkable accuracy improvement of 19.48 % was achieved at the 50-th percentile, while slightly lower improvements of 17.41 % and 6.23 % were obtained respectively for the 75-th and 95-th percentiles.

C. COMPARISON WITH EKF

To emphasize the superiority of the designed PF w.r.t. to the conventional EKF-based Bayesian position estimation, a worst-case comparison between the EKF used in [44] and the proposed PF is presented through their ECDF computed over the sector 4 shown in Figure 14. The PDF of the collaborative contributions in this case can be reasonably approximated through a Gaussian distribution and the motion is nearly-linear. Despite of EKF is expected to behave well in such specific nearly-ideal conditions the accuracy is still higher for the proposed Cognitive PF.

As shown in Figure 15 indeed, EKF showed remarkable positioning accuracy up to the 75-th percentile, and the

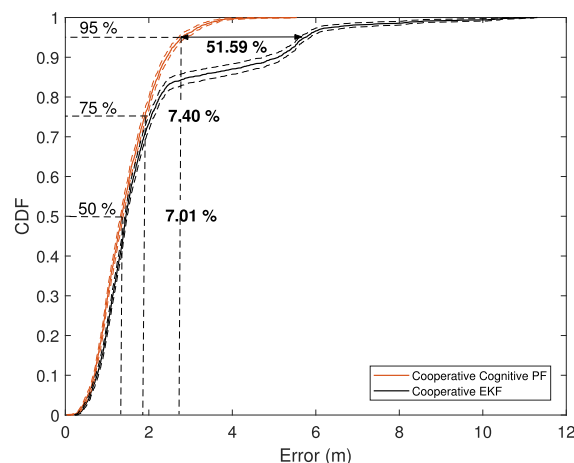


FIGURE 15. ECDF curve comparing the statistics of the position error for a target vehicle tightly integrating a single collaborative inter-agent distance in the prosed Cognitive PF and in a conventional hybridized EKF.

benefit provided by the cognitive PF is about the 7 % within a position error of 2 m. Differently, above the 75-th percentile, the accuracy of the PF overcome the EKF up to a maximum accuracy improvement of the 51.37 %.

VI. CONCLUSION

When GNSS-only CP is considered, PF can replace other Bayesian estimation filters such as EKF/UKF if a parallel architecture can be implemented to compensate for the increased complexity of the sequential filter [30]. The implementation of a PF is further motivated if an estimation of the noise probability distribution can be accurately performed about the input measurements (e.g. GNSS observables and inter-agent distances). Such estimated distributions can be used to dynamically build and use proper likelihood functions within the position estimation routine (i.e. particle weights computation). The results presented in this article show how an optimized PF using dynamic adaptation of both the covariance matrix involved in the particle generation and of the likelihoods used in the weight computation can achieve higher positioning accuracy w.r.t. suboptimal implementations investigated in previous works [30]. Furthermore, this study indirectly assessed that GEV distribution models is suitable for the generation of accurate likelihood functions required for the integration of collaborative ranging measurements, in the case they are computed through WLS-DD ranging. Further works shall address on-the-fly methods to dynamically estimate the statistics of collaborative range contributions for an actual implementation in the receiver architecture. In parallel it will be worth investigating the error on differential measurements when multi-constellation, multi-frequency code-based measurements are considered for the inter-agent distance estimation (i.e. Different-Frequency inter-system Mixed Double Difference (DFMDD)) [53].

REFERENCES

- [1] *Market Report: Issue 6*, GSA, GNSS Market Report, Washington, DC, USA, Oct. 2019.
- [2] A. Minetto, A. Nardin, and F. Dovis, "GNSS-only collaborative positioning among connected vehicles," in *Proc. 1st ACM MobiHoc Workshop Technol., Models, Protocols Cooperation Connected Cars TOP-Cars*, New York, NY, USA, 2019, pp. 37–42.
- [3] P. Popovski, K. F. Trillingsgaard, O. Simeone, and G. Durisi, "5G wireless network slicing for eMBB, URLLC, and mMTC: A communication-theoretic view," *IEEE Access*, vol. 6, pp. 55765–55779, 2018.
- [4] M. Alsenwi, N. H. Tran, M. Bennis, A. Kumar Bairagi, and C. S. Hong, "EMBB-URLLC resource slicing: A risk-sensitive approach," *IEEE Commun. Lett.*, vol. 23, no. 4, pp. 740–743, Apr. 2019.
- [5] A. Mukherjee, "Energy efficiency and delay in 5G ultra-reliable low-latency communications system architectures," *IEEE Netw.*, vol. 32, no. 2, pp. 55–61, Mar. 2018.
- [6] F. Shen, J. W. Cheong, and A. G. Dempster, "A DSRC Doppler/IMU/GNSS tightly-coupled cooperative positioning method for relative positioning in VANETs," *J. Navigat.*, vol. 70, no. 1, pp. 120–136, Jan. 2017.
- [7] I. Parvez, A. Rahmati, I. Guvenc, A. I. Sarwat, and H. Dai, "A survey on low latency towards 5G: RAN, core network and caching solutions," *IEEE Commun. Surveys Tuts.*, vol. 20, no. 4, pp. 3098–3130, 4th Quart., 2018.
- [8] *Using GNSS Raw Measurements on Android Devices*, GSA Working Group, Prague, Czech Republic, 2018.
- [9] U. Robustelli, V. Baiocchi, and G. Pugliano, "Assessment of dual frequency GNSS observations from a Xiaomi Mi 8 Android smartphone and positioning performance analysis," *Electronics*, vol. 8, no. 1, p. 91, Jan. 2019, doi: 10.3390/electronics8010091.
- [10] N. Gogoi, A. Minetto, N. Linty, and F. Dovis, "A controlled-environment quality assessment of Android GNSS raw measurements," *Electronics*, vol. 8, no. 1, p. 5, Dec. 2018, doi: 10.3390/electronics8010005.
- [11] A. Minetto and F. Dovis, "On the information carried by correlated collaborative ranging measurements for hybrid positioning," *IEEE Trans. Veh. Technol.*, vol. 69, no. 2, pp. 1419–1427, Feb. 2020.
- [12] J. Xiong, J. W. Cheong, Z. Xiong, A. G. Dempster, S. Tian, and R. Wang, "Integrity for multi-sensor cooperative positioning," *IEEE Trans. Intell. Transp. Syst.*, early access, Dec. 6, 2019, doi: 10.1109/TITS.2019.2956936.
- [13] A. I. Mourikis and S. I. Roumeliotis, "Performance analysis of multirobot cooperative localization," *IEEE Trans. Robot.*, vol. 22, no. 4, pp. 666–681, Aug. 2006.
- [14] S. I. Roumeliotis and G. A. Bekey, "Distributed multirobot localization," *IEEE Trans. Robot. Autom.*, vol. 18, no. 5, pp. 781–795, Oct. 2002.
- [15] R. Sharma, R. W. Beard, C. N. Taylor, and S. Quebe, "Graph-based observability analysis of bearing-only cooperative localization," *IEEE Trans. Robot.*, vol. 28, no. 2, pp. 522–529, Apr. 2012.
- [16] G. E. Garcia, L. S. Mupprisetty, E. M. Schiller, and H. Wymeersch, "On the trade-off between accuracy and delay in cooperative UWB localization: Performance bounds and scaling laws," *IEEE Trans. Wireless Commun.*, vol. 13, no. 8, pp. 4574–4585, Aug. 2014.
- [17] Y. Gao, S. Liu, M. M. Atia, and A. Noureldin, "INS/GPS/LiDAR integrated navigation system for urban and indoor environments using hybrid scan matching algorithm," *Sensors*, vol. 15, no. 9, pp. 23286–23302, 2015.
- [18] U. Niesen, V. N. Ekambaram, J. Jose, and X. Wu, "Intervehicle range estimation from periodic broadcasts," *IEEE Trans. Veh. Technol.*, vol. 66, no. 12, pp. 10637–10646, Dec. 2017.
- [19] Y. Zhou, C. L. Law, Y. L. Guan, and F. Chin, "Indoor elliptical localization based on asynchronous UWB range measurement," *IEEE Trans. Instrum. Meas.*, vol. 60, no. 1, pp. 248–257, Jan. 2011.
- [20] D. Yang, F. Zhao, K. Liu, H. B. Lim, E. Frazzoli, and D. Rus, "A GPS pseudorange based cooperative vehicular distance measurement technique," in *Proc. IEEE 75th Veh. Technol. Conf. (VTC Spring)*, May 2012, pp. 1–5.
- [21] J. Huang and H.-S. Tan, "A low-order DGPS-based vehicle positioning system under urban environment," *IEEE/ASME Trans. Mechatronics*, vol. 11, no. 5, pp. 567–575, Oct. 2006.
- [22] N. Alam, A. Tabatabaei Balaei, and A. G. Dempster, "A DSRC Doppler-based cooperative positioning enhancement for vehicular networks with GPS availability," *IEEE Trans. Veh. Technol.*, vol. 60, no. 9, pp. 4462–4470, Nov. 2011.
- [23] N. Alam, A. Tabatabaei Balaei, and A. G. Dempster, "Relative positioning enhancement in VANETs: A tight integration approach," *IEEE Trans. Intell. Transp. Syst.*, vol. 14, no. 1, pp. 47–55, Mar. 2013.
- [24] N. Alam and A. G. Dempster, "Cooperative positioning for vehicular networks: Facts and future," *IEEE Trans. Intell. Transp. Syst.*, vol. 14, no. 4, pp. 1708–1717, Dec. 2013.
- [25] B. Huang, Z. Yao, X. Cui, and M. Lu, "Dilution of precision analysis for GNSS collaborative positioning," *IEEE Trans. Veh. Technol.*, vol. 65, no. 5, pp. 3401–3415, May 2016.
- [26] M. L. D. Dardari and E. Falletti, *Satellite and Terrestrial Radio Positioning Techniques: A Signal Processing Perspective*. New York, NY, USA: Academic, 2012.
- [27] M. S. Arulampalam, S. Maskell, N. Gordon, and T. Clapp, "A tutorial on particle filters for online nonlinear/non-Gaussian Bayesian tracking," *IEEE Trans. Signal Process.*, vol. 50, no. 2, pp. 174–188, Feb. 2002.
- [28] R. Brown and P. Hwang, *Introduction to Random Signals and Applied Kalman Filtering With MATLAB Exercises*. Hoboken, NJ, USA: Wiley, 2012.
- [29] R. Zekavat and R. M. Buehrer, *Handbook of Position Location: Theory, Practice*, vol. 27. Hoboken, NJ, USA: Wiley, 2011.
- [30] A. Minetto, G. Falco, and F. Dovis, "On the trade-off between computational complexity and collaborative GNSS hybridization," in *Proc. IEEE 90th Veh. Technol. Conf. (VTC-Fall)*, Sep. 2019, pp. 1–5.
- [31] A. Doucet and A. M. Johansen, "A tutorial on particle filtering and smoothing: Fifteen years later," *Handbook Nonlinear Filtering*, vol. 12, nos. 656–704, p. 3, 2009.
- [32] D. Simon, *Optimal State Estimation: Kalman, H Infinity, and Nonlinear Approaches*. Hoboken, NJ, USA: Wiley, 2006.
- [33] F. Gustafsson, "Particle filter theory and practice with positioning applications," *IEEE Aerosp. Electron. Syst. Mag.*, vol. 25, no. 7, pp. 53–82, Jul. 2010.
- [34] T. Li, M. Bolic, and P. M. Djuric, "Resampling methods for particle filtering: Classification, implementation, and strategies," *IEEE Signal Process. Mag.*, vol. 32, no. 3, pp. 70–86, May 2015.
- [35] H. Zhou, Z. Yao, C. Fan, S. Wang, and M. Lu, "Rao-blackwellised particle filtering for low-cost encoder/INS/GNSS integrated vehicle navigation with wheel slipping," *IET Radar, Sonar Navigat.*, vol. 13, no. 11, pp. 1890–1898, Nov. 2019.
- [36] J. Georgy, A. Noureldin, M. J. Korenberg, and M. M. Bayoumi, "Low-cost three-dimensional navigation solution for RISS/GPS integration using mixture particle filter," *IEEE Trans. Veh. Technol.*, vol. 59, no. 2, pp. 599–615, Feb. 2010.
- [37] H. Xiong, R. Bian, Y. Li, Z. Du, and Z. Mai, "Fault-tolerant GNSS/SINS/DVL/CNS integrated navigation and positioning mechanism based on adaptive information sharing factors," *IEEE Syst. J.*, vol. 14, no. 3, pp. 3744–3754, Sep. 2020.
- [38] H. Xiong, J. Tang, H. Xu, W. Zhang, and Z. Du, "A robust single GPS navigation and positioning algorithm based on strong tracking filtering," *IEEE Sensors J.*, vol. 18, no. 1, pp. 290–298, Jan. 2018.
- [39] H. Qin, X. Xue, and Q. Yang, "GNSS multipath estimation and mitigation based on particle filter," *IET Radar, Sonar Navigat.*, vol. 13, no. 9, pp. 1588–1596, Sep. 2019.
- [40] Y. Shen and M. Z. Win, "Fundamental limits of wideband localization—Part I: A general framework," *IEEE Trans. Inf. Theory*, vol. 56, no. 10, pp. 4956–4980, Oct. 2010.
- [41] Y. Shen, H. Wymeersch, and M. Z. Win, "Fundamental limits of wideband localization—Part II: Cooperative networks," *IEEE Trans. Inf. Theory*, vol. 56, no. 10, pp. 4981–5000, Oct. 2010.
- [42] M. Z. Win, Y. Shen, and W. Dai, "A theoretical foundation of network localization and navigation," *Proc. IEEE*, vol. 106, no. 7, pp. 1136–1165, Jul. 2018.
- [43] A. Minetto, A. Nardin, and F. Dovis, "Tight integration of GNSS measurements and GNSS-based collaborative virtual ranging," in *Proc. 31st Int. Tech. Meeting Satell. Division Inst. Navigat. (ION GNSS+)*, Oct. 2018, pp. 2399–2413.
- [44] F. de Ponte Muller, E. M. Diaz, B. Kloiber, and T. Strang, "Bayesian cooperative relative vehicle positioning using pseudorange differences," in *Proc. IEEE/ION Position, Location Navigat. Symp. (PLANS)*, May 2014, pp. 434–444.
- [45] F. de Ponte Müller, A. Steingass, and T. Strang, "Zero-baseline measurements for relative positioning in vehicular environments," in *Proc. 6th Eur. Workshop GNSS Signals Signal Process.*, 2013, p. 10. [Online]. Available: <https://elib.dlr.de/86457/>
- [46] E. Kaplan and C. Hegarty, "Understanding GPS/GNSS: Principles and applications," in *GNSS Technology and Applications*. Norwood, MA, USA: Artech House, 2017.

- [47] M. Tahir, S. S. Afzal, M. S. Chughtai, and K. Ali, "On the accuracy of inter-vehicular range measurements using GNSS observables in a cooperative framework," *IEEE Trans. Intell. Transp. Syst.*, vol. 20, no. 2, pp. 682–691, Feb. 2019.
- [48] O. Hlinka, F. Hlawatsch, and P. M. Djuric, "Distributed particle filtering in agent networks: A survey, classification, and comparison," *IEEE Signal Process. Mag.*, vol. 30, no. 1, pp. 61–81, Jan. 2013.
- [49] S. Coles, J. Bawa, L. Trenner, and P. Dorazio, *An Introduction to Statistical Modeling of Extreme Values*, vol. 208. Cham, Switzerland: Springer, 2001.
- [50] A. Gurrieri, "Integration of cooperative GNSS measurements by particle filter, master thesis," Ph.D. dissertation, Politecnico di Tori, Turin, Italy, 2020.
- [51] F. Gustafsson, F. Gunnarsson, N. Bergman, U. Forssell, J. Jansson, R. Karlsson, and P.-J. Nordlund, "Particle filters for positioning, navigation, and tracking," *IEEE Trans. Signal Process.*, vol. 50, no. 2, pp. 425–437, Aug. 2002.
- [52] R. Douc and O. Cappe, "Comparison of resampling schemes for particle filtering," in *Proc. 4th Int. Symp. Image Signal Process. Anal. (ISPA)*, 2005, pp. 64–69.
- [53] G. Li, J. Wu, C. Zhao, and Y. Tian, "Double differencing within GNSS constellations," *GPS Solutions*, vol. 21, no. 3, pp. 1161–1177, Jul. 2017.



ALEX MINETTO (Member, IEEE) was born in Pinerolo, Italy, in 1990. He received the B.Sc. and M.Sc. degrees in telecommunications engineering from the Politecnico di Torino, Turin, Italy, and the Ph.D. degree in electrical, electronics, and communications engineering in 2020. He joined the Department of Electronics and Telecommunications, Politecnico di Torino, in 2019, as a Research and Teaching Assistant. In 2015, he spent a six-month internship at European Organization for the Exploitation of Meteorological Satellites (EUMETSAT), Darmstadt, Germany. His current research interests include signal processing and advanced Bayesian estimation applied to global navigation satellite system (GNSS) cooperative receivers.



ALESSANDRO GURRIERI was born in Grottaglie, Italy, in 1993. He received the master's degree from the NavSAS Research Group, Turin, Italy, and the M.Sc. degree in communications and computer networks engineering in 2020. His research interest includes navigation filter for GNSS-based collaborative positioning methods.



FABIO DOVIS (Member, IEEE) was born in Bruino, Italy, in 1970. He received the M.Sc. and Ph.D. degrees from the Politecnico di Torino, Turin, Italy, in 1996 and 2000, respectively. In 2004, he joined the Department of Electronics and Telecommunications, Politecnico di Torino, as an Assistant Professor. Since 2014, he has been an Associate Professor with the Department of Electronics and Telecommunications, Politecnico di Torino, where he coordinates the Navigation Signal Analysis and Simulation (NavSAS) Research Group. He has a relevant experience in European projects in satellite navigation as well as cooperation with industries and research institutions. His research interests include the design of GPS and Galileo receivers and advanced signal processing for interference and multipath detection and mitigation, as well as ionospheric monitoring. He serves as a member of the IEEE Aerospace and Electronics Systems Society Navigation Systems Panel.

• • •